LAWRENCE
LIVERMORE
NATIONAL
LABORATORY

LLNL-TR-815543

Replacing photomultiplier tubes with silicon photomultipliers for nuclear safeguards applications

K. Kazkaz, T. Stiegler

October 12, 2020

Disclaimer

This work performed under the auspices of the U.S. Department of Energy by Lawrence Livermore National Laboratory under Contract DE-AC52-07NA27344.

Replacing photomultiplier tubes with silicon photomultipliers for nuclear safeguards applications

K. Kazkaz
LLNL, kareem@llnl.gov

T. Stiegler
LLNL, stiegler1@llnl.gov

ABSTRACT

Photomultiplier tubes (PMTs) have been used for decades as the default light detection technology for scintillator-based radiation monitors. PMTs come with a handful of disadvantages, however, including large volume usage, fragility, high-voltage requirements, and susceptibility to magnetic fields. Arrays of silicon photomultipliers (SiPMs) are a possible alternative to PMTs providing similar performance while offering improvements in the areas listed. We focus on straightforward "drop-in replacement" evaluations by imposing a single channel output of the SiPM signal and a backend electronics data acquisition and analysis routine identical to that used for PMTs. In the realm of nuclear safeguards, the primary performance metric for gamma spectroscopy is detector resolution, and for neutron detection it is pulse shape discrimination (PSD) to separate neutron and gamma signals. In this work we present the results of replacing a PMT with a 2" x 2" SiPM array mounted, in turn, to the same 2" x 2" cylindrical sodium iodide (NaI) crystal. The ultimate comparison for this gamma spectrometry is confirmation of uranium enrichment standards, ranging from depleted uranium to 93% highly enriched uranium (HEU), by analyzing the resulting spectra with both a simple integral scaling in key energy regions of the spectrum, as well as with the NaIGEM software package. In addition to the gamma spectroscopy work, we will present the latest results on comparing the PSD capabilities of a 4" x 4" SiPM array to a 5" PMT. As with the gamma spectroscopy evaluations, the light detectors are mounted in turn to the same liter-scale organic scintillators. This neutron-focused work includes evaluation of prototype SiPM readout boards with a single output signal summed over 256 individual SiPM pixels, and evident tradeoffs between PSD capability and fast response.

INTRODUCTION

International nuclear safeguards instrumentation[1] relies on well-established technology to increase the reliability of survey results. Within the catalog of this instrumentation we find scintillator-based detectors with mounted photomultiplier tubes (PMTs), which have been the main photodetection workhorse for scintillator-based gamma and neutron detection for decades[2]. Although the technology has undergone continual improvements, the fundamental technology remains the same: an evacuated glass volume with internal structure to amplify the signal from the incident photons (see Fig. 1).

PMTs have disadvantages that are inextricably linked to the basic design. These disadvantages include

- Dimensions typically larger than the scintillator volume itself
- Fragility related to the glass construction and the need to maintain a high-quality vacuum within the body of the device
- Susceptibility to magnetic fields that disrupt the required amplification paths between the dynodes
- Temperature dependence that affects photocathode charging
- High voltage requirement, typically on the order of 900 - 1500 V

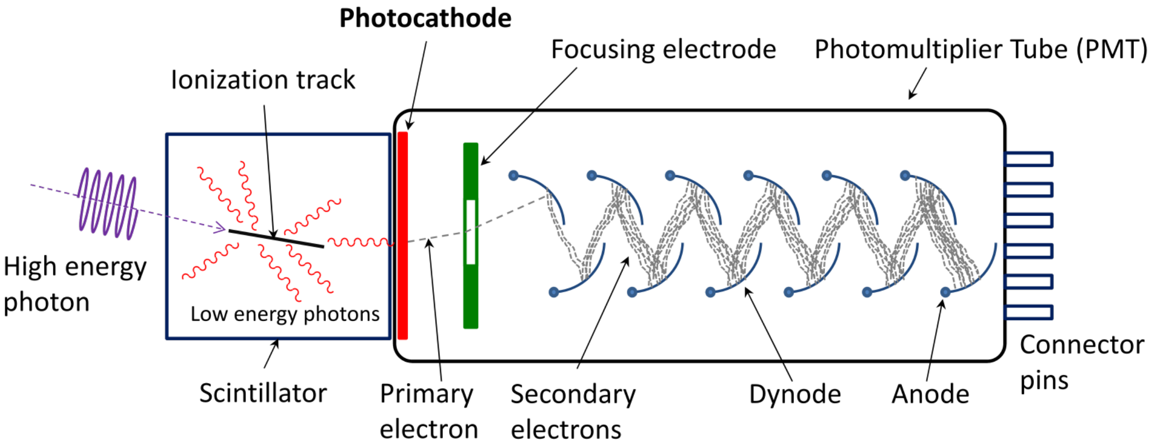

Figure 1. The basic operation of scintillator-based radiation detection. The photomultiplier tube extends from the photocathode to the connector pins, and consists of an evacuated glass volume with internal dynodes to electrically amplify the signal from the incident photons. Unaltered image used under auspices of the Creative Commons[3].

Despite these and other recognized disadvantages, PMTs have strong advantages including:

- Single-channel readout, though multi-channel PMTs also exist
- Low-current power requirements, typically 50 μA or less
- Single power supply
- Fast response, ~20 ns return to baseline output levels for a single photoelectron
- High dynamic range, typically over two orders of magnitude
- High degree of linearity over the dynamic range
- Low cost per unit, US$1-1.5K for the kinds of PMTs used in safeguards instrumentation

To address the disadvantages of PMTs, Kazkaz and Swanberg conducted a scoping study[4] to evaluate commercial and near-commercial technology as replacements for PMTs. The replacement technology was evaluated in terms of addressing the listed disadvantages while maintaining the recognized advantages. The technology with the clearest promise to be a viable PMT replacement was an array of silicon photomultipliers (SiPMs).

Based on this conclusion, in this work we embark on a direct comparison of PMT and SiPM performance within the context of nuclear safeguards technology. Our comparisons focus on both gamma spectroscopy and its applicability to uranium enrichment measurements, as well as fast neutron detection for material characterization.

Note that for these comparisons, we are not necessarily attempting to maximize the performance of the entire system, but merely to compare the PMT and SiPM results. It may be possible, by using different backend electronics to increase resolution or enhanced pulse shape analysis to better separate the neutron and gamma signals, to improve the performance of one system or the other. Likewise, we could devise custom packaging to minimize volume usage. While we take some steps in these directions, these optimizations are not the driving goal of the current work. We wish to evaluate the performance of a PMT-based system to a SiPM-based one, while keeping all other aspects of the apparatus and analysis chains as unchanged as possible. This allows us to compare the PMT and SiPM results directly, and make the most robust conclusions possible about replacement viability.

GAMMA SPECTROSCOPY AND URANIUM ENRICHMENT MEASUREMENTS

The first comparison we performed that is relevant to nuclear safeguards is the measurement of uranium enrichment levels. We utilized a set of uranium enrichment standards from New Brunswick Laboratory, Certified References Materials 146 and 969[5]. These standards were all approximately 200 g of compressed U_3O_8 material, with enrichments varying from depleted uranium to 93% highly enriched. To make the evaluation more relevant to field use, we also used four shielding configurations, from no shielding to 5/8” steel plate. Table I shows the full list of configuration variables. The key hardware components are shown in Fig. 2, with details available in Table II. Optical grease was used to couple each photodetector to the NaI crystal.

Table I. Experimental setup variables. We acquired a dataset for every permutation shown in this table, resulting in 56 datasets. In addition, we acquired periodic background and calibration datasets to ensure data quality. The stated enrichments are the mass ratio of ^{235}U to total uranium content.

Parameter	**Values**
Photodetector	PMT, SiPM
Shielding	None, 1/4” steel, 1/2” steel, 5/8” steel
Enrichment	0.32% (depleted), 0.71% (natural), 2.95%, 4.46%, 20.1%, 52.5%, 93.2%

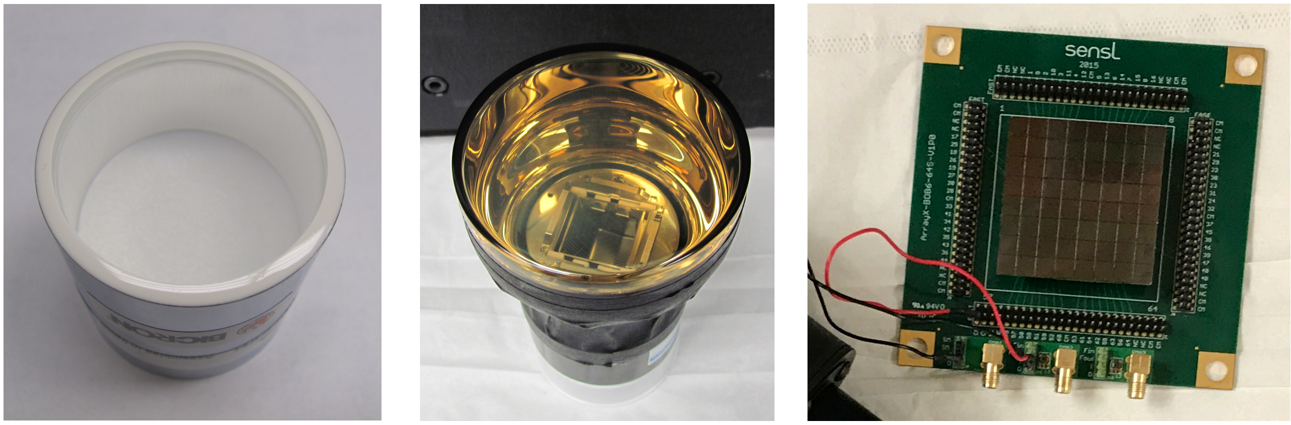

Figure 2. The key components in the gamma spectroscopy and uranium enrichment measurements are, left to right: the 2” × 2” sodium iodide crystal, the 3” PMT, and the SiPM array. The active area of the SiPM, visible as the dark square in the center of the printed circuit board with the smaller graduated squares, measured 2” × 2”. The SiPM readout board measured 4” × 4”.

Table II. Details of the key hardware components of the gamma spectroscopy / uranium enrichment study. The alternative SiPM readout board from AiT was used after the main data campaign to study the effects of an alternative readout on the quality of the SiPM-based data.

Component	Model
Sodium iodide crystal	2” × 2” right cylinder, Saint Gobain SA-12428
PMT	Hamamatsu R6233-100 SEL
SiPM array	On Semiconductor ARRAYJ-60035-64P-PCB
SiPM readout board	On Semiconductor ArrayX-BOB6-64S
Alternative SiPM readout board	AiT Instruments AB1DVM

Datasets were acquired for each permutation of the physical setup shown in Table 1. The required livetime was 300 seconds for no shielding, 600 seconds for the 1/4” steel plate, and 900 seconds for the 1/2” and 5/8” plates. Fig. 3 shows an example of a physical setup. The data acquisition chain after the photodetector was an Ortec 113 preamplifier, an Ortec 570 amplifier, and an Ortec 927 analog-to-digital converter with pulse heights recorded within the Ortec Maestro software.

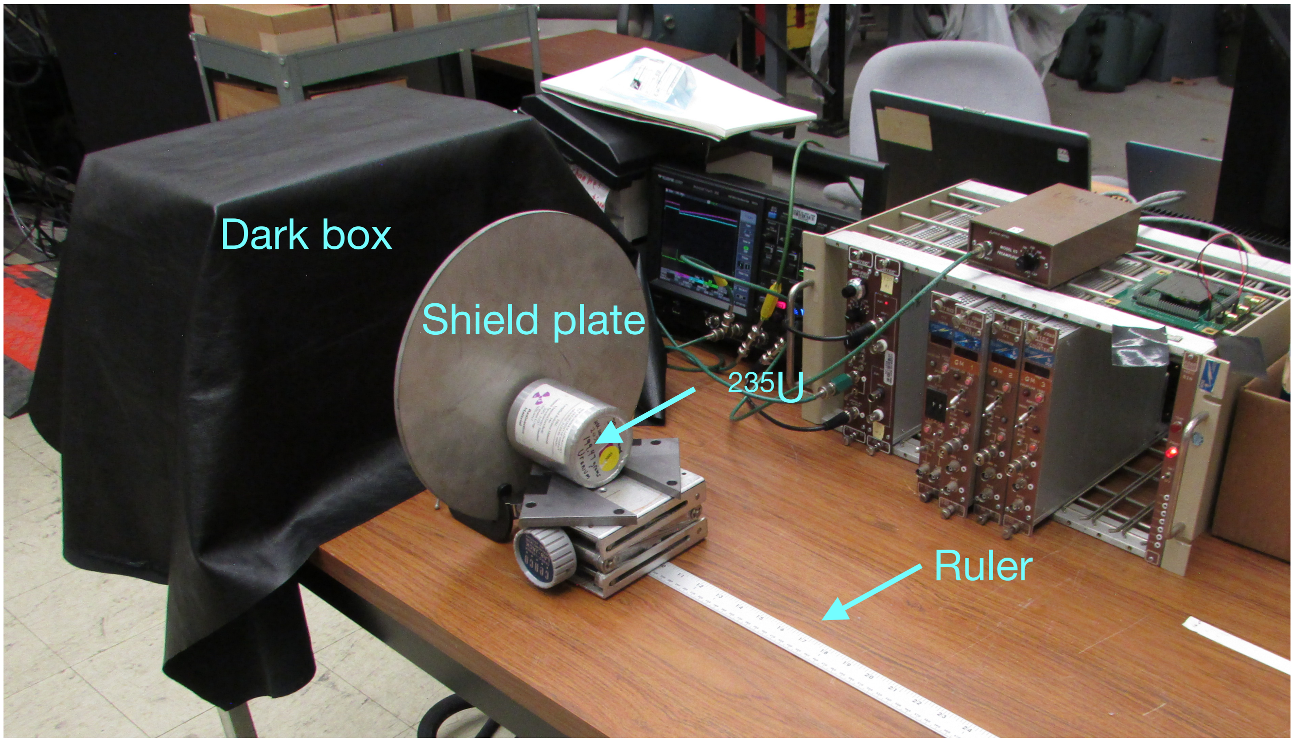

Figure 3. Typical experimental setup. A ruler was used to reproduce placement of the shield and source. The scintillator system was located inside the dark box.

The most intense gamma lines from ^{235}U and ^{238}U are at 186 keV and 1001 keV, respectively. To ensure proper calibration for both these gamma rays, we used sources with gamma emission bracketing this range. Specifically, we used ^{241}Am (59 keV), ^{137}Cs (662 keV), and ^{60}Co (1173 keV and 1332 keV). All three sources were used simultaneously to provide a single calibration spectrum, and the source distances were set to provide approximately equivalent significance in their respective peaks. Fig. 4 shows the resulting spectra from two calibration runs, one with the PMT mounted to the NaI crystal, and the other with the SiPM mounted to the same crystal.

The calibration peaks show the PMT and SiPM to have very similar performance in terms of resolution across the relevant energy range. We noted, however, that the SiPM displayed greater nonlinearity in response, necessitating a multi-point, higher-order calibration to ensure data reliability. Table III shows the measured resolutions of three of the calibration peaks.

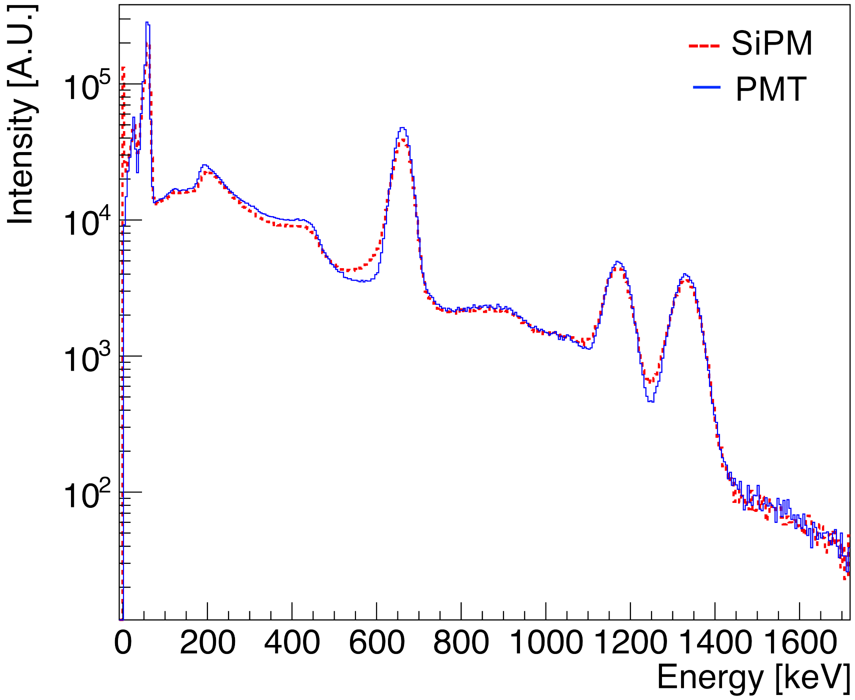

Figure 4. Calibration spectra for the SiPM and the PMT, with ^{241}Am, ^{137}Cs, and ^{60}Co sources present. Each peak in the PMT spectrum is slightly narrower than the corresponding peak in the SiPM dataset, though the difference is small enough to neglect in the context of nuclear safeguards gamma spectroscopy. In some situations (e.g., with a lone ^{137}Cs source), the SiPM-mounted NaI exhibited a narrower peak than the PMT-mounted NaI. The continuum background model used around each peak could also reorder the slight relative performance increase between the SiPM and the PMT.

Table III. Full-width at half-maximum resolutions of the two photodetectors at various energies. In this case the PMT resolution is uniformly a little better than the resolution with the SiPM, although we found that taking the calibration data under different conditions, e.g., with individual sources, greater dead time, or a different fit model for the underlying background continuum, the SiPM-mounted detector displayed narrower peaks than the PMT-mounted detector.

Peak energy (keV)	PMT resolution (%)	SiPM resolution (%)
59	10.5 ± 0.11	14.13 ± 0.14
662	6.72 ± 0.03	7.08 ± 0.03
1332	5.00 ± 0.03	5.26 ± 0.04

With the detectors calibrated, we turned our attention to the uranium enrichment datasets. Fig. 5 shows spectra from the PMT and SiPM. We performed two analyses of the data to verify uranium enrichment levels. The first was developed by Sprinkle et al., a simple scaling of the number of counts in two key regions of the spectrum: one around the 186-keV peak, and a second on the high-energy side of that same peak[6]. The second approach was to use the NaIGEM software, which simultaneously fits predefined curves to the spectrum in 186 keV region.

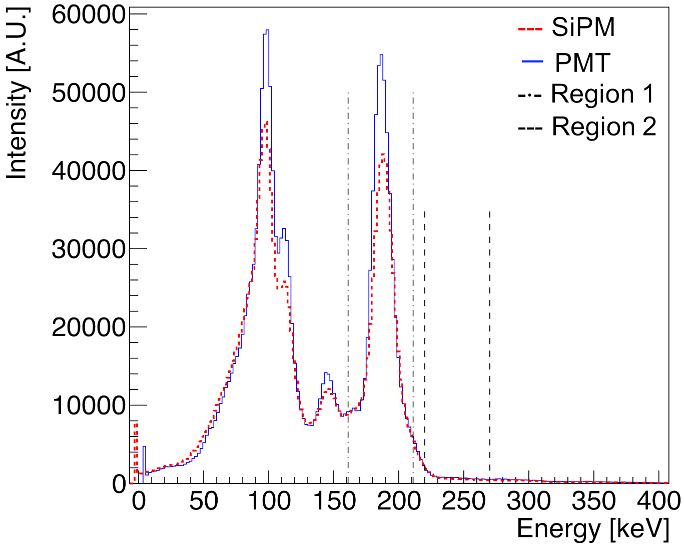

Figure 5. SiPM-based and PMT-based uranium spectra. This dataset was specifically of the 93% enriched data with no shielding. The two defined regions are for use in Sprinkle et al.'s scaling method for determining enrichment levels. The apparent difference in peak heights stem from energy-dependent bin widths in the two histograms related to the nonlinear energy calibrations. The analysis relies on the integration of bin heights within the regions, rather than a fit curve, thus the apparent difference in peak heights does not affect the final outcome.

In the Sprinkle approach, a simple linear equation is used to define the enrichment of a sample:

$$E = a \cdot S1 + b \cdot S2 \tag{1}$$

where *E* is the enrichment level, *S1* and *S2* are the integrated counts in regions 1 and 2 respectively, and the coefficients *a* and *b* are fit parameters. This approach requires a minimum of two datasets to establish the values of *a* and *b*. One systematic effect based on natural statistical fluctuations comes from extrapolating to values outside the range of the calibration, therefore we used the depleted and 93% enriched uranium datasets for the calibration. Because we used only two points in the calibration, recalculating the enrichment of the calibration data would give exact results—a situation that will never be encountered in the field. We can, however, apply the calibration to the

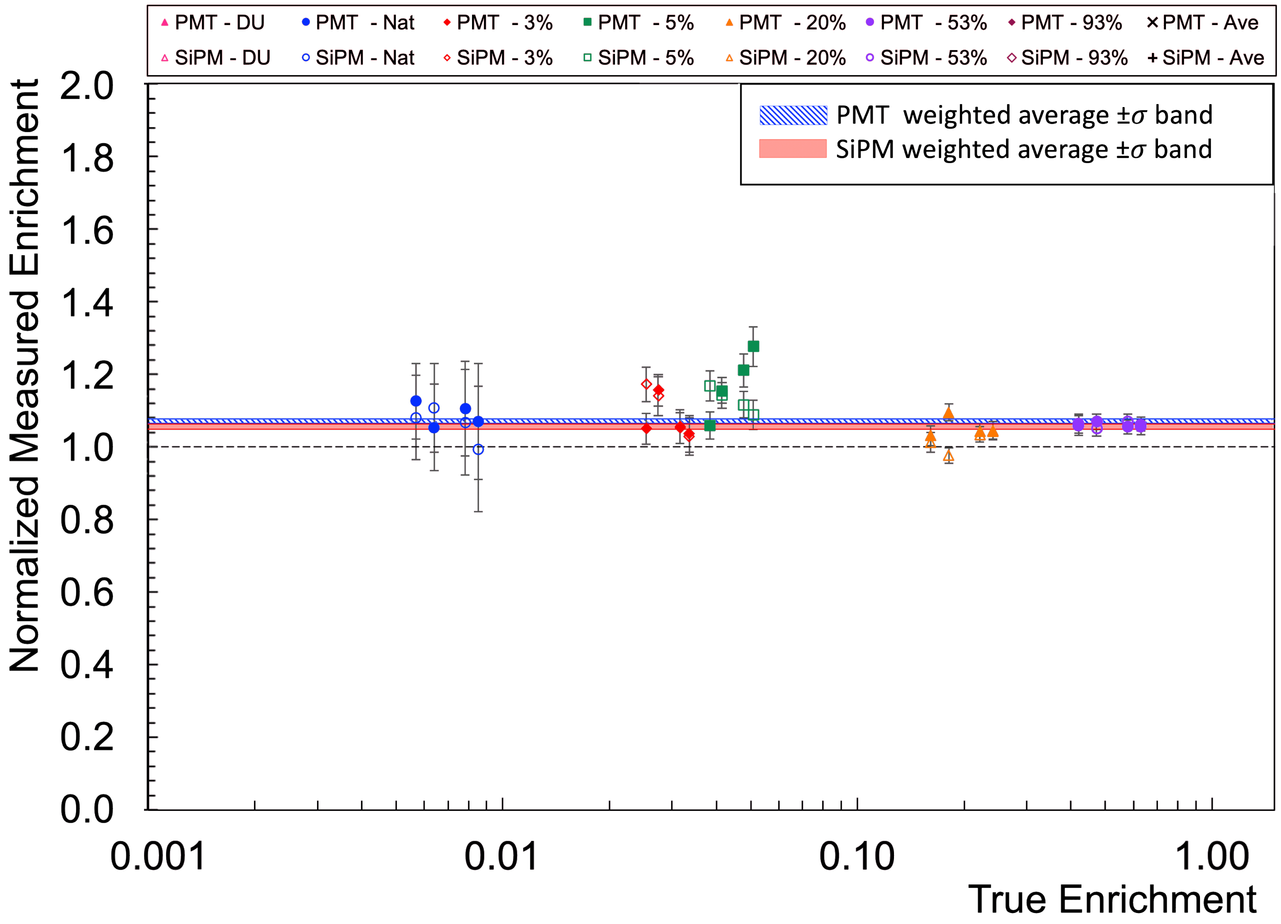

Figure 6. Results of the Sprinkle et al. method for determining uranium enrichment levels. We see that the PMT and SiPM data are overlapping, leading us to conclude similar performance between the two photodetectors.

five intermediate datasets, with results shown in Fig. 6, which plots the ratio of the measured enrichment to the known enrichment, for each of the four shielding configurations and five enrichment levels. Each data grouping (i.e., blue, red, green, orange and purple datapoints) represents an individual enrichment, an artificial spread has been applied for better visual clarity. We fit a constant value across all points, weighted by the uncertainties, to obtain an overall accuracy for the PMT- and SiPM-mounted detector. The results are shown in Table IV.

Improvement on the accuracy was attempted by fitting Eq. 1 across all enrichment levels,, but systematic scattering and shielding effects resulted in an average value 7% lower than expectation, as opposed to the 7% overestimate using just two enrichments. We conclude the two-point calibration is preferable since was also the approach taken by Sprinkle et al.

The NaIGEM[7] analysis was performed with version 2.1.4. NaIGEM fits curves to the region surrounding the 186-keV peak, and the constraints result in more accurate results than Sprinkle et al. NaIGEM requires a single calibration dataset to tune the energy scale, enrichment level, and effects of the shielding. The fitting routines and additional analysis within the software, however, allow for a quasi-independent analysis of the calibration dataset such that the returned results do not identically match the input. We were therefore able to analyze all seven enrichment levels.

In working with the NaIGEM software, we discovered it was very sensitive to the starting values for the fit parameters. If we were not methodical about the steps used, we would obtain inconsistent results (e.g., an energy calibration on any given dataset might change, depending on the previous energy calibration). We ultimately settled on the following protocol:

Table IV. Accuracy of the SiPM- and PMT-based data for the uranium enrichment measurements. Quoted value is a weighted average across all enrichments and shielding configurations. The simple scaling approach has a systematic relative offset of 6-7%. The NaIGEM analysis gets closer to the expected enrichment values, with a relative offset of 2%. Regardless of which analysis routine is used, the PMT and SiPM results are within 2σ with the simple scaling approach, and 1σ when using the NaIGEM software. We therefore conclude a PMT and a SiPM array exhibit comparable performance for the purposes of uranium enrichment studies.

Photodetector	Simple scaling	NaIGEM
PMT	1.070 ± 0.007	1.022 ± 0.012
SiPM	1.056 ± 0.007	1.017 ± 0.005

1. Open each datafile in PeakEasy and rebin the data to ensure 1024 channels in the full spectrum.
2. Perform a linear calibration of the 20% enrichment dataset within any given photodetector / shielding configuration using the 186-keV (^{235}U), 1460-keV (background ^{40}K), and 2615-keV (background ^{208}Tl) peaks. Record the zero offset and gain values.
3. Set the shielding thickness in the NaIGEM window (Fig. 7) to the nominal value. This field requires a non-zero value for proper operation, so for the data acquired with no shield a value of 1 ± 1 mm was used.
4. Perform the energy and width calibration within NaIGEM on the 20% enrichment data using the values recorded in step 2 as the starting values.
5. Perform the enrichment calibration within NaIGEM using the 20% enrichment data.
6. Perform the absorber calibration within NaIGEM using the 20% enrichment data.
7. Analyze all seven datasets within the photodetector / shielding configuration without any additional energy, width, enrichment, or absorber calibrations.

The results of any given NaIGEM analysis are displayed in a window that shows the fit curves as well as a quality-of-fit parameter, as depicted in Fig. 8. The results of the full NaIGEM analysis are

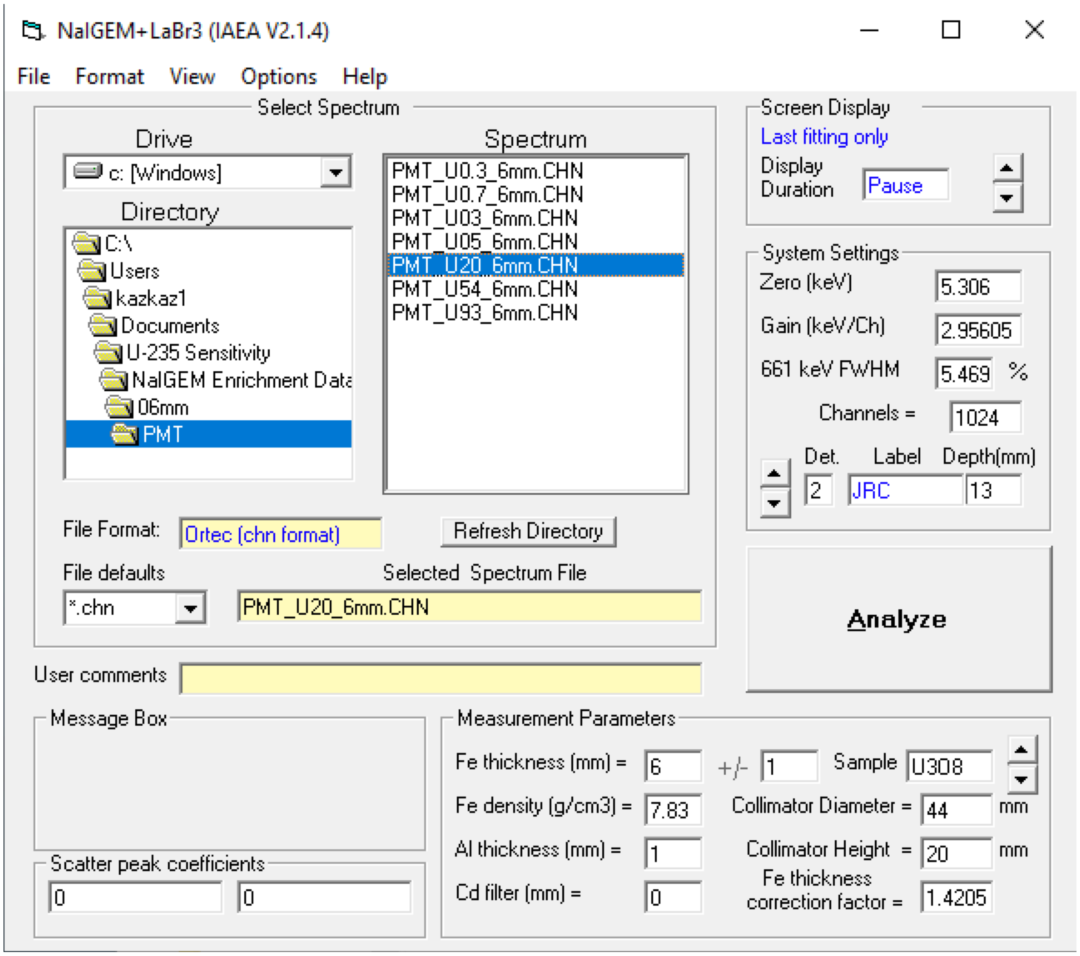

Drive: c: [Windows]

Directory:
C:\
Users
kazkaz1
Documents
U-235 Sensitivity
NaIGEM Enrichment Data
06mm
PMT

Spectrum:
PMT_U0.3_6mm.CHN
PMT_U0.7_6mm.CHN
PMT_U03_6mm.CHN
PMT_U05_6mm.CHN
PMT_U20_6mm.CHN
PMT_U54_6mm.CHN
PMT_U93_6mm.CHN

File Format: Ortec (chn format)
File defaults: *.chn
Selected Spectrum File: PMT_U20_6mm.CHN
User comments:

Screen Display: Last fitting only
Display Duration: Pause

Zero (keV): 5.306
Gain (keV/Ch): 2.95605
661 keV FWHM: 5.469 %
Channels = 1024
Det.: 2
Label: JRC
Depth(mm): 13

Fe thickness (mm) = 6 +/- 1
Sample: U3O8
Fe density (g/cm3) = 7.83
Collimator Diameter = 44 mm
Al thickness (mm) = 1
Collimator Height = 20 mm
Cd filter (mm) = 0
Fe thickness correction factor = 1.4205

Scatter peak coefficients: 0 0

Figure 7. Primary NaIGEM control window for version VB 2.1.4. Starting fit values must be entered in the fields along the right and bottom of the window.

shown in Fig. 9. The NaIGEM results are less precise than the region scaling approach, but they are also more accurate. Within the NaIGEM analysis, we conclude that the PMT and SiPM return very comparable results, supporting the notion that SiPMs are indeed a viable replacement for PMTs for the purposes of uranium enrichment determination via gamma spectroscopy. Results are included in Table IV.

As a final study of the SiPM gamma spectroscopy performance, and mindful of possible volume minimization, we obtained a second SiPM readout board, this one from AiT Instruments, model

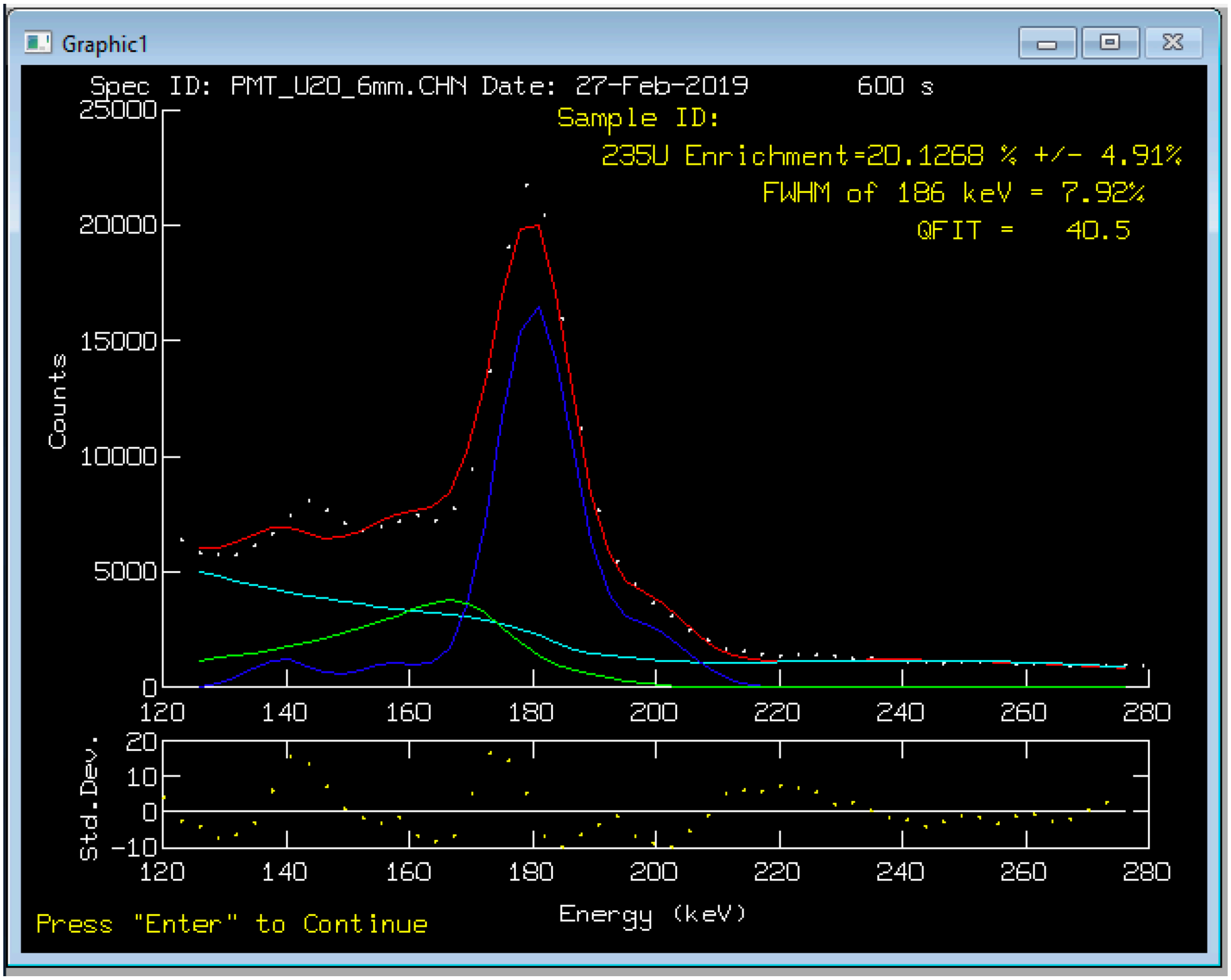

```
Spec ID: PMT_U20_6mm.CHN Date: 27-Feb-2019       600 s
                              Sample ID:
                                235U Enrichment=20.1268 % +/- 4.91%
                                       FWHM of 186 keV = 7.92%
                                              QFIT =    40.5
```

```
Press "Enter" to Continue
```

Figure 8. NaIGEM fit window. The enrichment as mass percentage and relative uncertainty are reported in the upper right, along with a quality-of-fit parameter. The atomic percentage enrichment are reported on a subsequent text screen. The reported uncertainty is a relative value, not an absolute value.

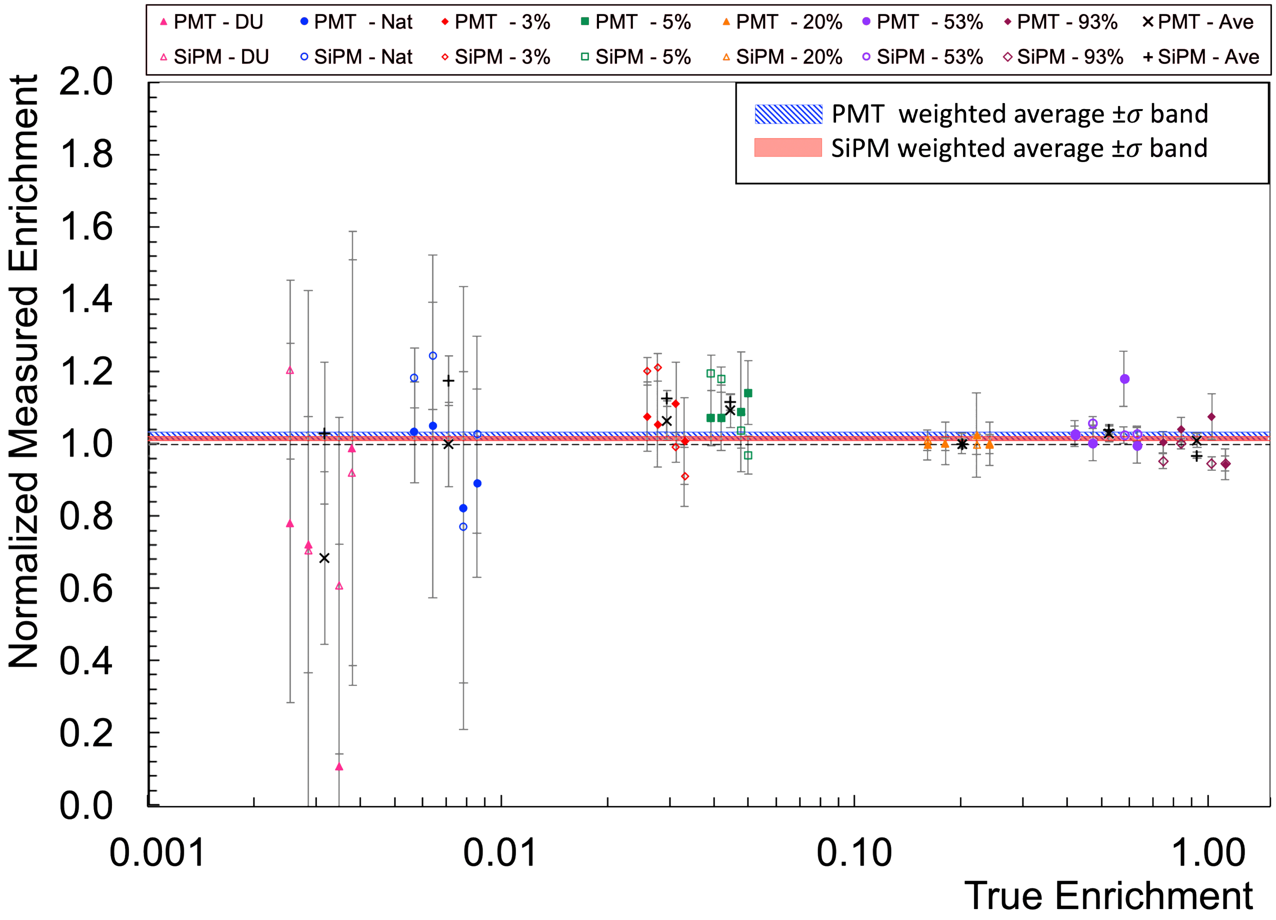

Figure 9. Results of the NaIGEM analysis for determining uranium enrichment levels. As with the region scaling approach of Sprinkle et al., *we* see that the PMT and SiPM data are overlapping. In this plot, we also included within each data grouping the weighted average and standard deviation, shown by the crosses (PMT data) and plusses (SiPM data).

AB1DVM (see Table II). The AiT readout board measures approximately 2” × 2”, so it is much closer in size to the SiPM array itself.

The AiT readout board has a faster response and return to baseline than the On Semi readout board, as shown in Fig. 10. The board also has notably worse resolution than either the On Semi readout board or the PMT, as shown in Fig. 11. The lesson from this study is that the SiPM readout board can have a strong impact on the performance of the SiPM, and the most appropriate readout board must be selected for any given application.

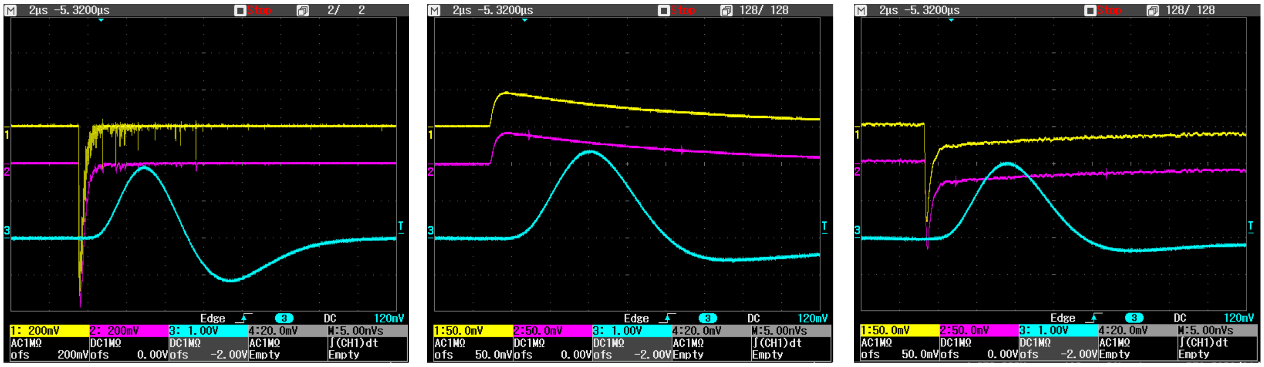

Figure 10. Pulses from the PMT (left), SiPM with On Semi readout (center), and SiPM with AiT readout (right). For each image, the yellow curve is the raw pulse, the purple is the signal after pre-amplification, and the blue pulse is from the amplifier. The amplified PMT pulse shows clear dipolar response. The SiPM response is mostly unipolar with both readouts, but we see that the response of the AiT readout is much sharper in time than the On Semi readout.

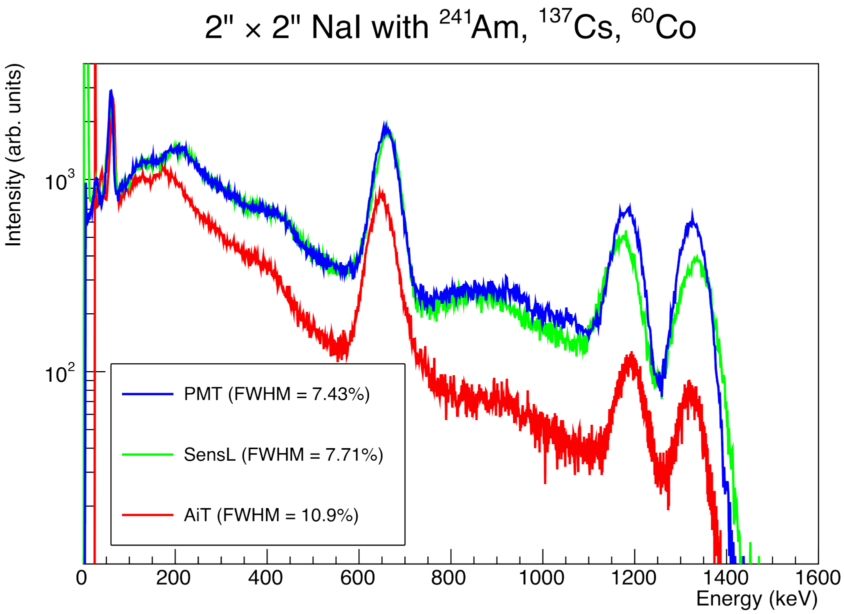

Figure 11. Calibration spectra from the PMT and the SiPM array with either the On Semi (SensL) or AiT readout board. While the AiT readout board has much quicker response than the On Semi board (see Fig. 10), the full-width at half-maximum resolution of the AiT board at 662 keV is notably larger (10.9%) than either the PMT (7.4%) or the SiPM read out with the On Semi board (7.7%).

FAST NEUTRON DETECTION AND PULSE SHAPE ANALYSIS

In addition to gamma spectroscopy, PMTs have been commonly used to instrument scintillators for neutron detection. These scintillators are usually of an organic material that is capable of pulse shape discrimination (PSD), where the light pulse has a time signature that depends on whether the incident particle was a gamma or a neutron. Because fission neutrons are typically emitted in a strong background of gamma rays, the quality of the discrimination between gammas and neutrons is a key performance metric.

The practice of pulse shape analysis (PSA) is well established. The most common approach relies on determining how much of the light from a scintillator occurs near the beginning of a pulse, and how much light lasts to later times. Fig. 12 graphically shows a notional pulse from a neutron detector, and how the pulse can be analyzed to achieve pulse shape discrimination. Because the scintillation decay constants are on the order of 100 ns, fast response from the photodetector is of paramount importance—if the photodetector spreads out every pulse in time, it degrades the pulse shape capabilities of the underlying scintillator material. We therefore evaluated SiPMs as PMT replacements in the context of neutron detection, where PSD and timing are more important than resolution and spectroscopy.

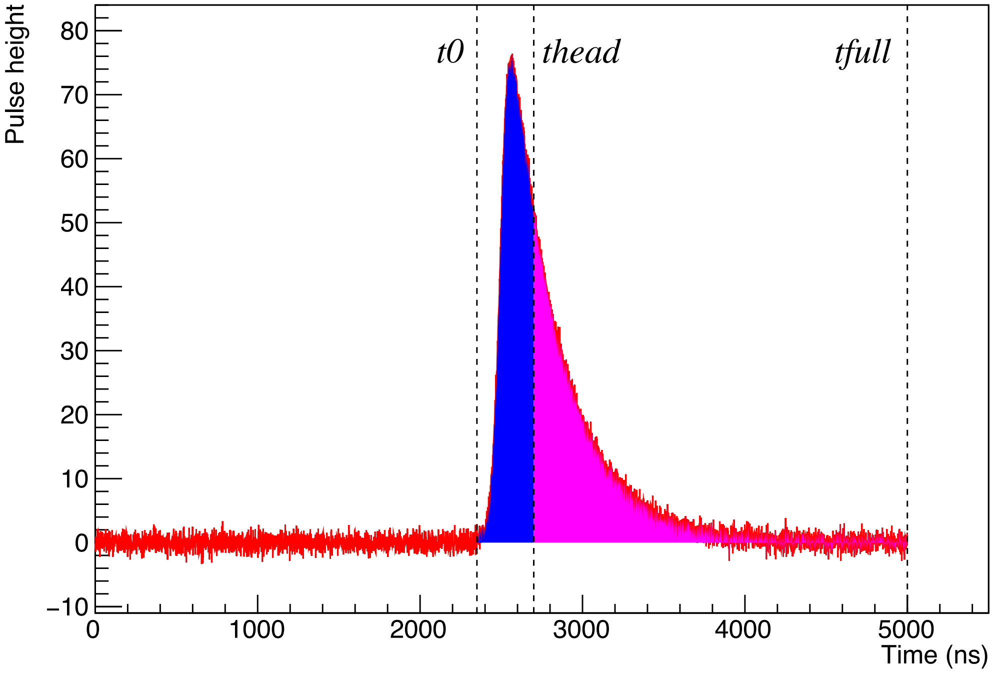

Figure 12. Notional neutron pulse. Pulse shape discrimination is achieved by taking a ratio of the tail of the pule (the magenta area) to the full pulse (the blue plus magenta areas). We optimized the values of *t0* and *thead* in our analysis.

The basic experimental program mirrors that of the gamma spectroscopy comparison: obtain PSD data with a PMT mounted to a neutron detector, replace the PMT with a SiPM array on the same neutron detector, and compare the results. To make the comparison more relevant to a wider selection of instrumentation, we compared PMT and SiPM PSD performance for three neutron detection scintillators: the organic crystal stilbene, the liquid scintillator EJ-309, and the PSD-capable plastic EJ-299-33M. Still in the spirit of maintaining PMT advantages, we worked with AiT Instruments to develop a single-channel, single-power-supply readout board that can be populated with 4 SiPM arrays, to create an active area of 4” × 4”, and thus comparable in area to a 5” PMT. The photodetector output was connected directly to a CAEN 1730 digitizer. The basic experimental hardware and setup are shown in Fig. 13 with details given in Table V.

We calibrated the detectors using three gamma sources—^{241}Am (60 keV), ^{137}Cs (662 keV), and ^{22}Na (511 keV and 1275 keV)—to account for the nonlinear response from the SiPM arrays. Because the organic scintillators have low photopeak efficiency, we ran a series of GEANT4 simulations[8] to

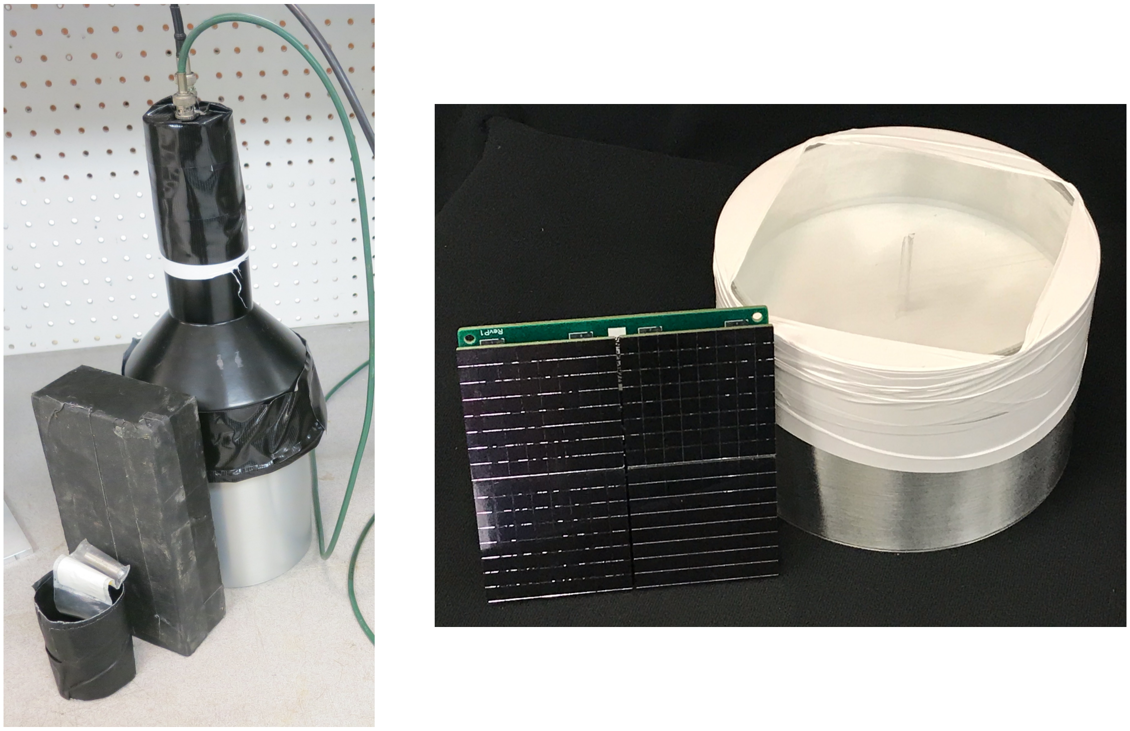

Figure 13. Hardware used in the evaluation of PSD capabilities of a SiPM array, as compared to a PMT. The photo on the left shows a ^{252}Cf fission source, a 2” lead shield, and the PMT mounted on a scintillator with 5” diameter. The eventual data used in the comparison was acquired with an 8” lead shield to reduce the gamma rate. The photo on the right shows the 4” × 4” SiPM array mounted to a readout board with a single channel output, and a 5” scintillator with Teflon tape mask.

Table V. Details of the key hardware components of the neutron detection / PSD study. Each neutron detector was 5” in diameter, although the heights differed. Only one SiPM readout board, from AiT Instruments, exists that can accommodate four 2” × 2” SiPM arrays.

Component	Model
Organic crystal scintillator	5” dia × 3” high stilbene, Inrad Optics
Liquid scintillator	5” dia × 5” high EJ-309, Eljen Tech.
PSD-capable plastic scintillator	5" dia × 5" high EJ-299-33M, Eljen Tech.
PMT	5” dia, Hamamatsu HS6527
SiPM and readout	On Semiconductor ARRAYJ-60035-64P-PCB
SiPM readout	AiT Instruments AB1TS4

identify features in the calibration energy spectra (see Fig. 14). The three simulations were of the three calibration sources, and the decays were generated using the GEANT4 Radioactive Decay Manager, which emits alpha and beta particles as well as the gamma rays. The simulations therefore included a source capsule volume to contain the charged particles.

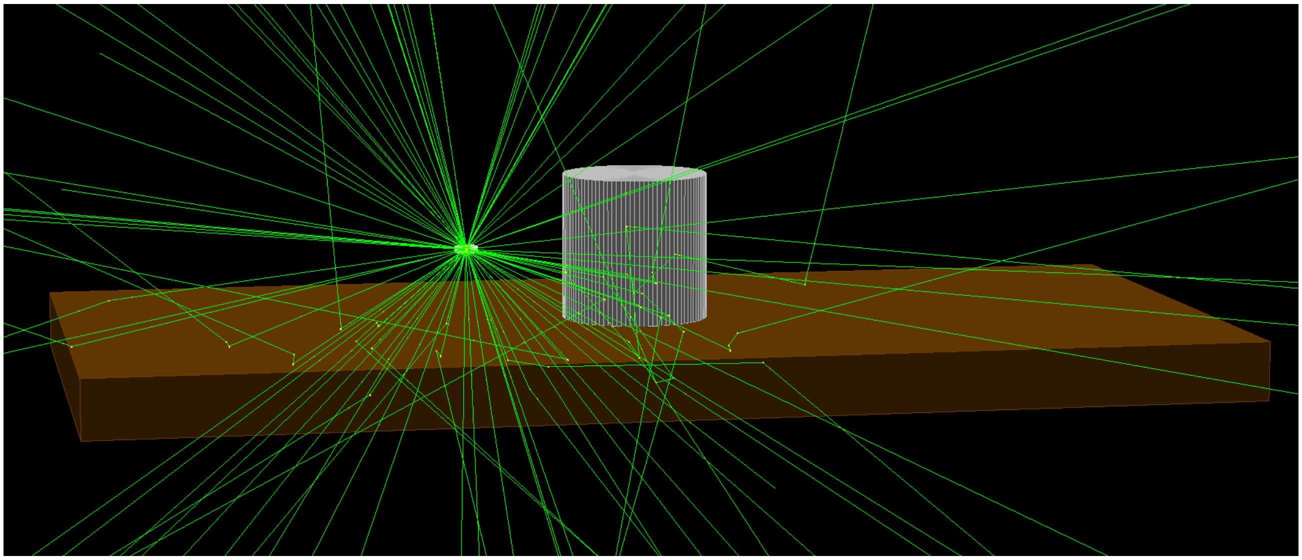

Figure 14. Image of the geometry present in the GEANT4 simulation of the 5” × 5” EJ-309 neutron detector (white cylinder) and the ^{137}Cs source (emitting gamma rays, here colored green). The brown table surface was included to account for scattered interactions. The simulation was used to identify features in the experimental gamma calibration spectra.

The gain of the experimental data and the width of the simulated data was adjusted for each combination until the spectra showed reasonable overlap (see Fig. 15). Because of the high statistics and the limited fidelity of the simulation, as well as the lack of a detector response module, the gains and widths were evaluated by using an iterative approach rather than an analytical approach. Once the energy-dependent gain and width were determined, empirical fits were applied to create

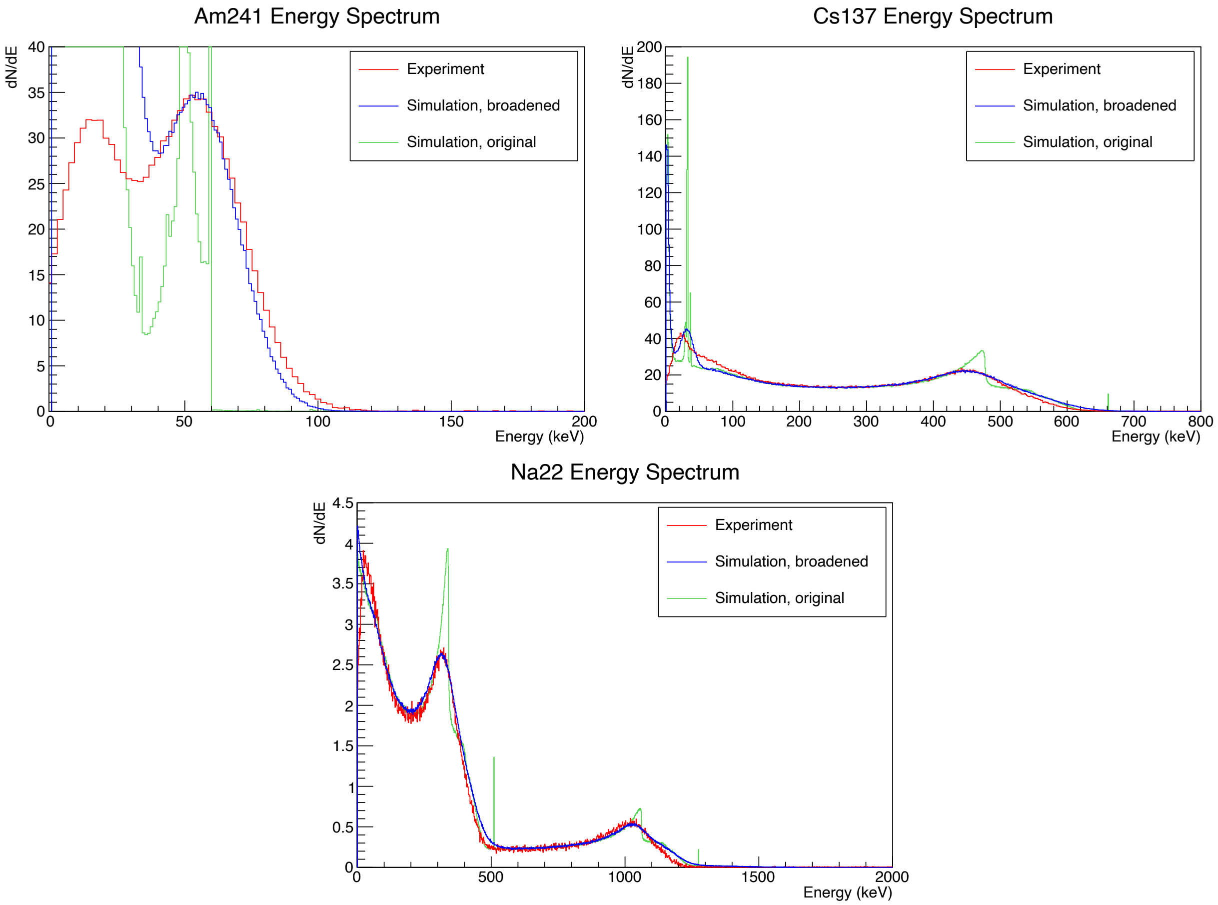

Figure 15. Comparison of simulation and experimental ^{241}Am, ^{137}Cs, and ^{60}Co calibration spectra. For each of these plots, the raw simulated spectrum is shown in green. The simulated spectra had an energy-dependent width applied to broaden the peaks until they matched the width of the experimental data. Simultaneously, the experimental data was scaled in a nonlinear fashion until the experimental peaks matched the simulation peaks. Note that the peak centroids have suppressed energies relative to both the photopeak (in the case of the ^{241}Am calibration) and the Compton edges (in the cases of the ^{137}Cs and ^{60}Co calibrations). This effect is attributed to peak broadening combined with stronger tails on the low-energy side of the feature edges.

smooth, analytic response curves. The empirical energy and width calibrations, with fit parameters *p0*, *p1*, and *p2*, are given by the equations, with the fits shown in Fig. 16.

$$\text{Energy calibration factor} = p0 + p1\ exp\left(-\frac{E}{p2}\right) \tag{2}$$

$$\text{Width calibration factor} = p0 + p1\ \left(1 - exp\left(-\frac{E}{p2}\right)\right) \tag{3}$$

After performing the energy and width calibrations, we turned our attention to a rough optimization of the pulse shape analysis parameters *t0* and *thead*. For a given pulse, we calculate the ratio of the area in the tail (magenta area in Fig. 12) to the full area of the peak (blue plus magenta areas in Fig. 12). This ratio is the pulse shape parameter. The energy of the pulse is the full integral, calibrated using Eq. [2]. We then take these value pairs of pulse shape parameter and energy to create scatter plots, shown in Fig. 16. For a given energy region in this scatter plot, we create a histogram of the events, and fit two Gaussian curves to the neutron and gamma bands (Fig. 16). The PSD Figure of Merit (FOM) is a measure of the separation of the Gaussian peaks, and is given by

$$\text{Figure of Merit} = \frac{|C_1 - C_2|}{\sigma_1 + \sigma_2} \tag{4}$$

where C_1, C_2, σ_1, and σ_2 are the fit centroids and widths of the two peaks, as obtained from the fits shown in the bottom image of Fig. 16.

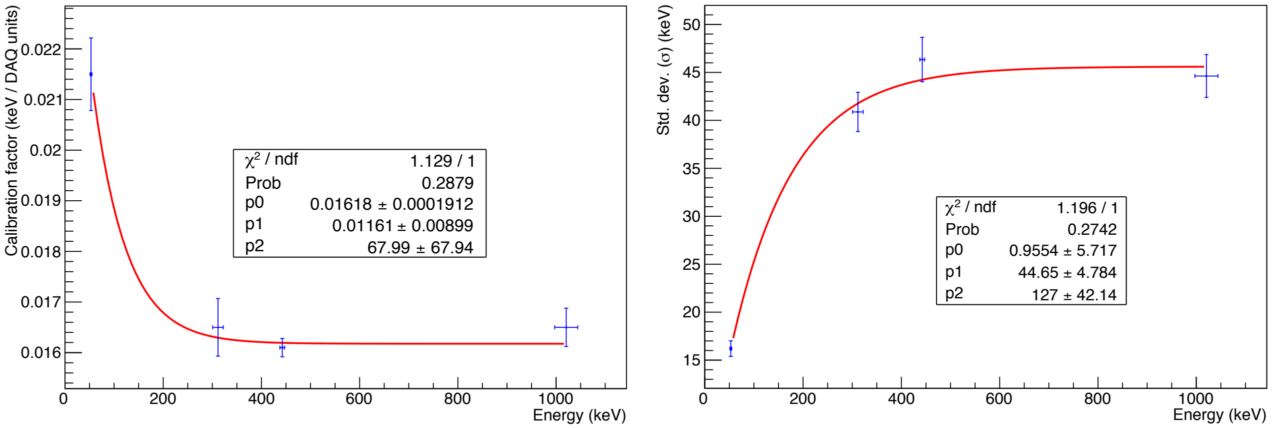

Figure 16. Empirical fits to the energy (left) and width (right) calibrations of the EJ-309 detector. Calibrations were performed with gamma sources, so the eventual energy is expressed in units of keV electron-equivalent.

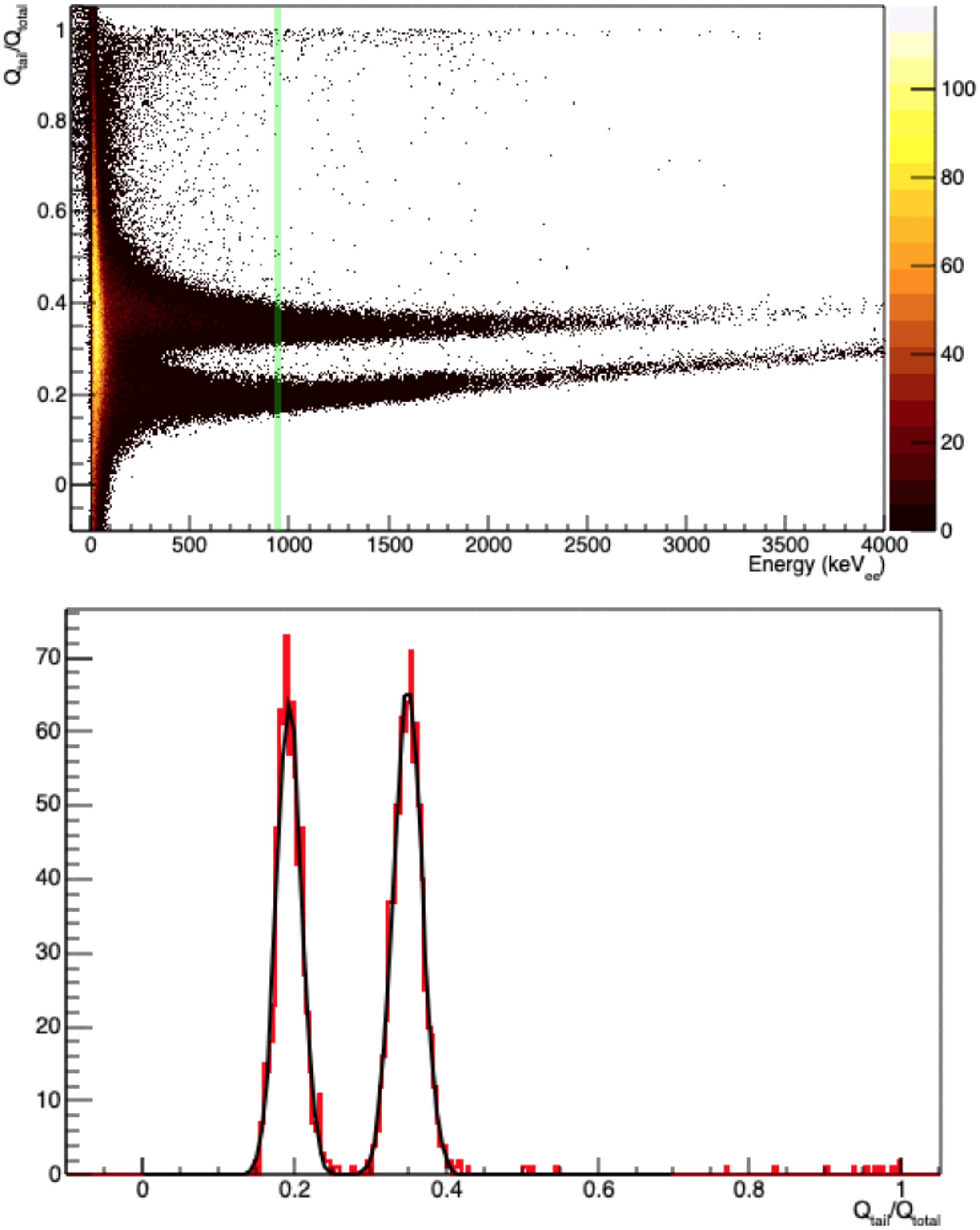

Figure 17. Results of the pulse shape analysis. The top image is a scatter plot of the pulse shape parameter (vertical axis) and the calibrated energy (horizontal axis). The two prominent bands are the neutron and gamma signals. By taking a slice of data in energy, shown in the top image by the vertical green band, we can create a histogram of the events, shown in the bottom image. Fitting two Gaussian curves to the data gives us both the centroids and widths of the peaks.

The energy slice is shown by the green band in the top image of Fig. 17. We calculate the FOM for each slice while stepping across the full range, with the results plotted in Fig. 18. Note that the FOM calculation breaks down when the number of events in either band becomes too low to obtain a reliable fit. This instability becomes noticeable between 2000 and 2500 keV, with a complete breakdown between 2500 and 3000 keV, though acquiring additional data would extend the onset of instability to higher energies.

For the region of stability, we fit a smooth curve to the data, and calculate the maximum value of that curve. That maximum fit FOM is determined for a broad range of both *t0* and t*head*, with results plotted in Fig. 19. Within that figure we see a strong diagonal band of near-maximal FOM, along with a much more vertical band. We take the optimized pulse shape parameters to be at the apex of the diagonal and vertical bands. For the PMT-based data, those parameters were consistently found to be *t0* = 2350 ns, and *thead* = 90 ns. The optimal value of *t0* is based primarily on the location of the trigger within the recorded pulse, which was set to be near the center of the 5000-ns-long digitization frame, which explains the band with the negative slope: the crucial parameter to set is the location of the division between early light and late light properly within the

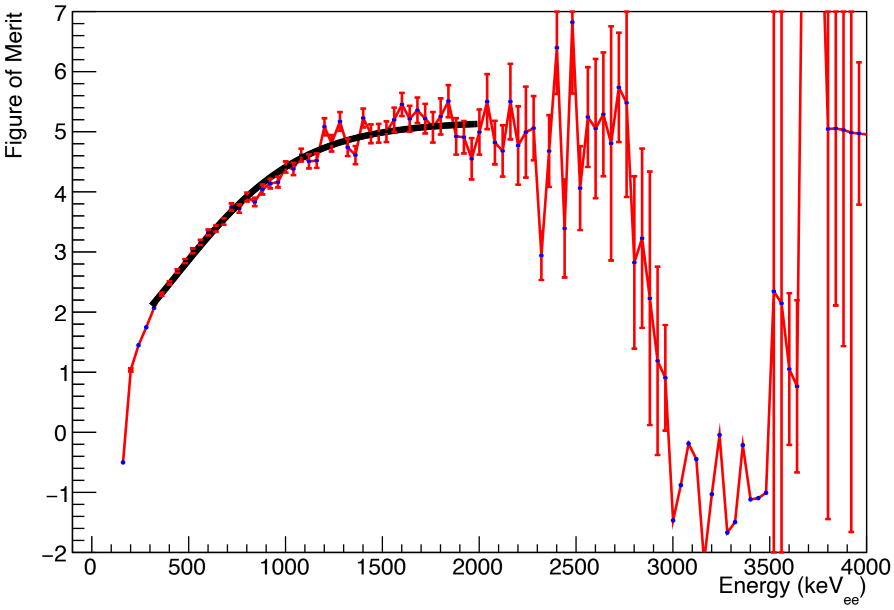

Figure 18. Figure of Merit and fit for one set of pulse shape parameters. The fit is the smooth black curve fit between 300 and 2000 keV. We calculate the maximum value of this fit curve within the fit range to determine the optimal pulse shape parameters.

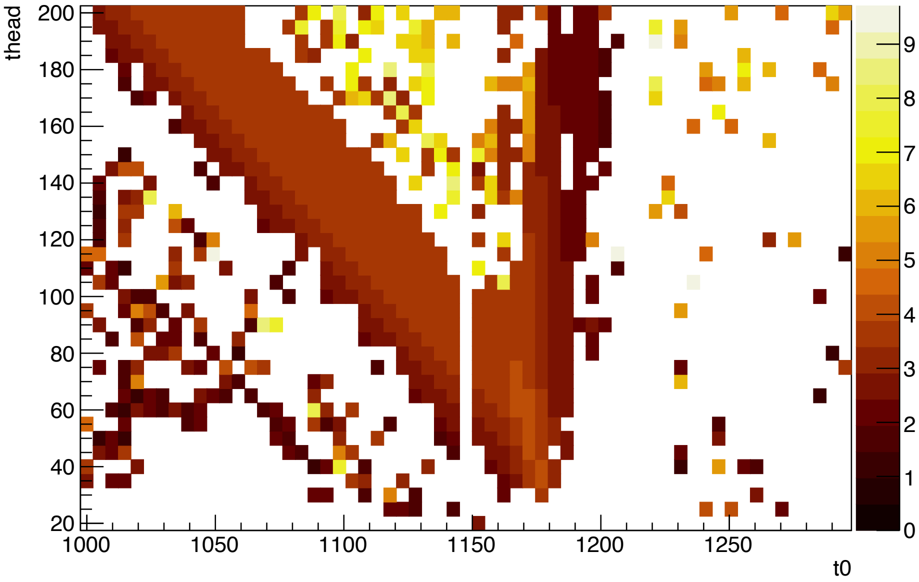

Figure 19. Optimization of the pulse start and the dividing line between the early light and the late light. The units are given in digitizer clock ticks, which in this case was 2 ns. The *t0* parameter therefore runs between 2000 and 2600 ns, while *thead* runs between 40 and 400 ns. The maximum Figure of Merit was the highest separation between the neutron and gamma bands (see Fig. 17). While the maximum Figure of Merit occurs outside these strong bands, that comes from poor reconstruction of the Gaussian curves in cases where the bands are not clearly distinguished, and thus they are not considered to give proper optimal settings for the pulse shape parameters.

pulse itself. Thus the optimal division within our data acquisition set points occurs at 2440 ns on an absolute scale, regardless of where the pulse integration begins.

Fig. 20 shows the PSD scatter plots and FOM curves for the datasets with the PMT mounted to the three neutron detector cylinders. From these plots, we see that the best detector is the stilbene (FOM = 6.6), followed by the EJ-309 (FOM = 5.2), then the EJ-299-33M (FOM = 3.8).

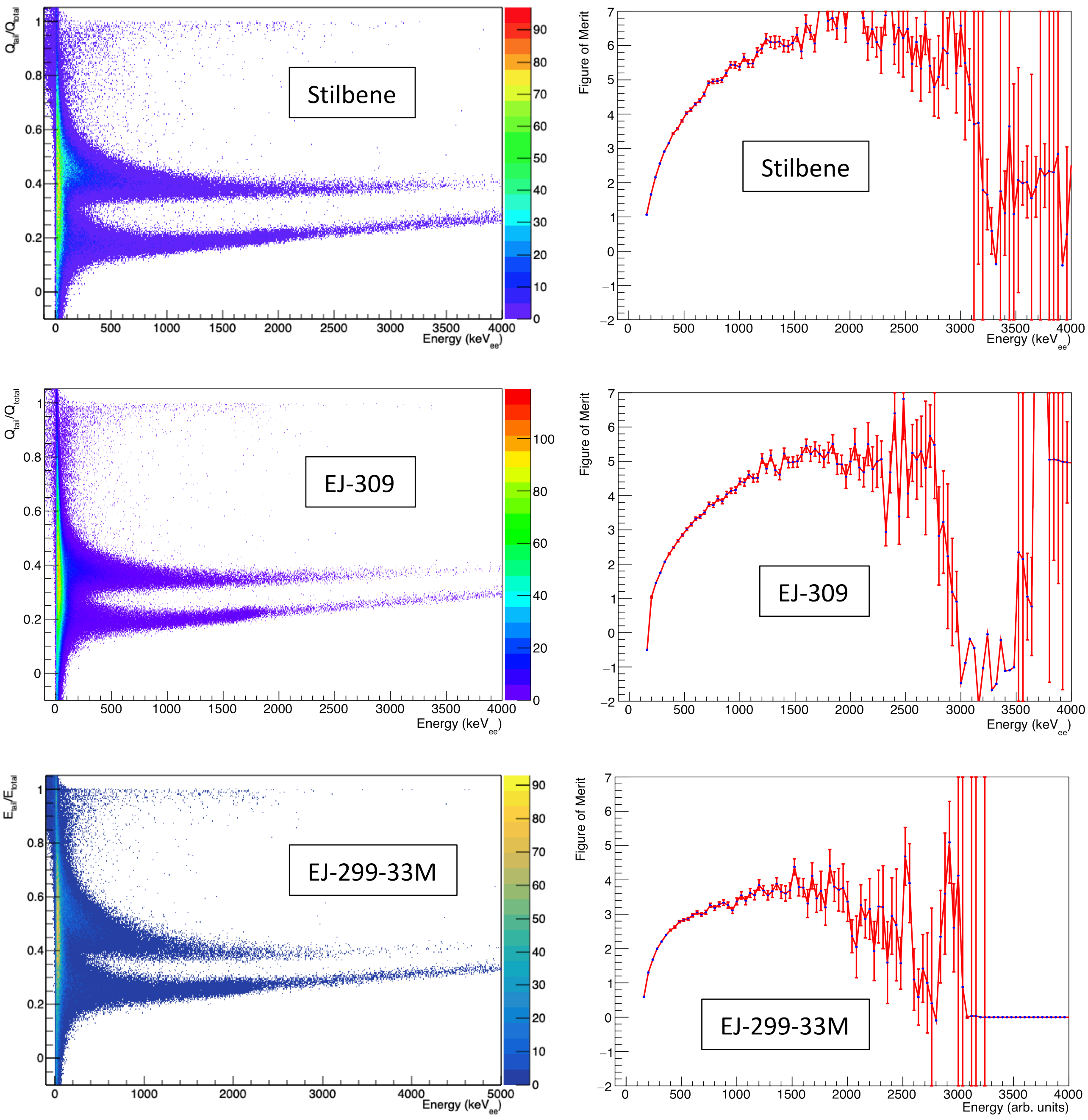

Figure 20. PSD performance of three neutron detection materials instrumented with a PMT. The left column shows the energy spectrum of the events, with the pulse shape parameter plotted on the vertical axis, allowing for a clean separation of the neutron and gamma bands. The column on the right is the Figure of Merit, which is a measure of how well-separated those bands are. The best performance comes from the stilbene detector (FOM = 6.6), followed by the EJ-309 (FOM = 5.2), then the EJ-299-33M (FOM = 3.8).

We then turned our attention to the SiPM-mounted detectors. We obtained both cylindrical and square detectors for this comparison. The EJ-309 and EJ-299-33M cylinders measured 5” in diameter and 5” high, while the stilbene cylinder was 5” diameter and 3” high. The square detectors all outer dimensions of 4x4x3 in^3. We characterized the noise levels of the SiPM array mounted to the cylindrical stilbene detector to compare to the PMT performance, with the results shown in Fig. 21. The baseline noise levels of the SiPM array are more than a factor of 2 larger than the noise levels of the PMT, which will broaden the gamma and neutron PSD bands. The board manufacturer, AiT Instruments, also identified a long tail (Fig. 22) resulting from a short, 5-ns laser pulse to the SiPM array. Since the PSD analysis relies on a ratio of late light to total light, this further serves to reduce the difference between gamma and neutron recoils. Both the excess noise and the long tail reduces the separation between the gamma and neutron bands and increases the overall tail / total ratio, as shown in Fig. 23. Even given these differences in performance, the optimal PSD parameters were largely unchanged between from those of the PMT-mounted detectors, and the optimization plots showed the same features as visible in Fig. 19.

While the SiPM data from this configuration shows degraded performance relative to the PMT, we do not believe this to be an underlying physics limitation. Other groups have demonstrated clear PSD capabilities from SiPMs mounted to stilbene crystals, though those efforts have been

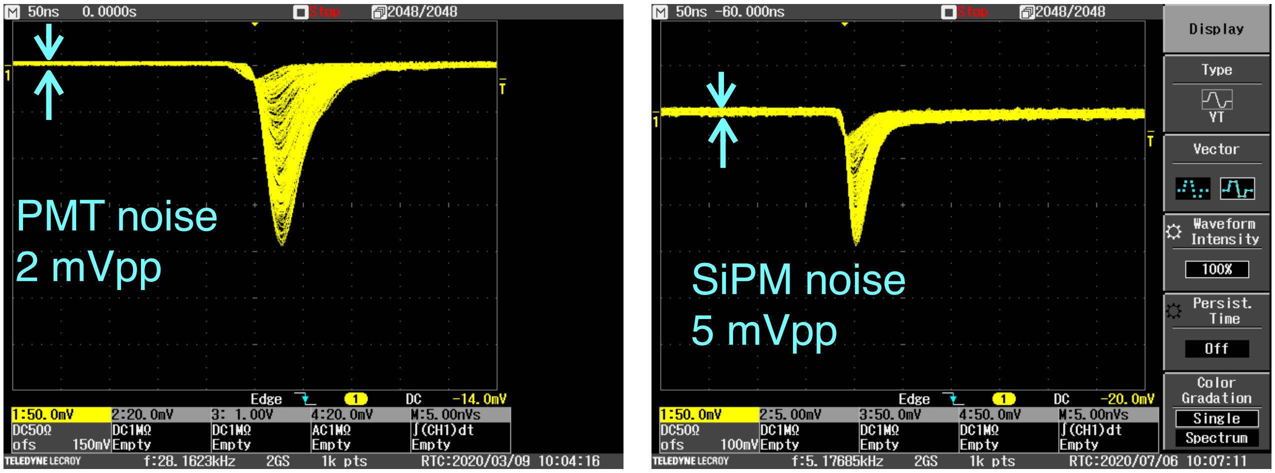

Figure 21. Baseline noise of the PMT (left) and the 4” × 4” SiPM array (right) mounted to the stilbene detector. We used a ^{137}Cs source to provide the pulses, and the bias of both the PMT and SiPM array were set to provide pulses roughly 150 mV in amplitude. The baseline noise levels of the PMT are approximately 2 mV peak-to-peak, while the SiPM array read out with the AiT Instruments AB1TS4 board had a peak-to-peak noise of approximately 5 mVpp. This noise partly obscured the late light emitted by the stilbene detector, degrading the PSD performance of the SiPM.

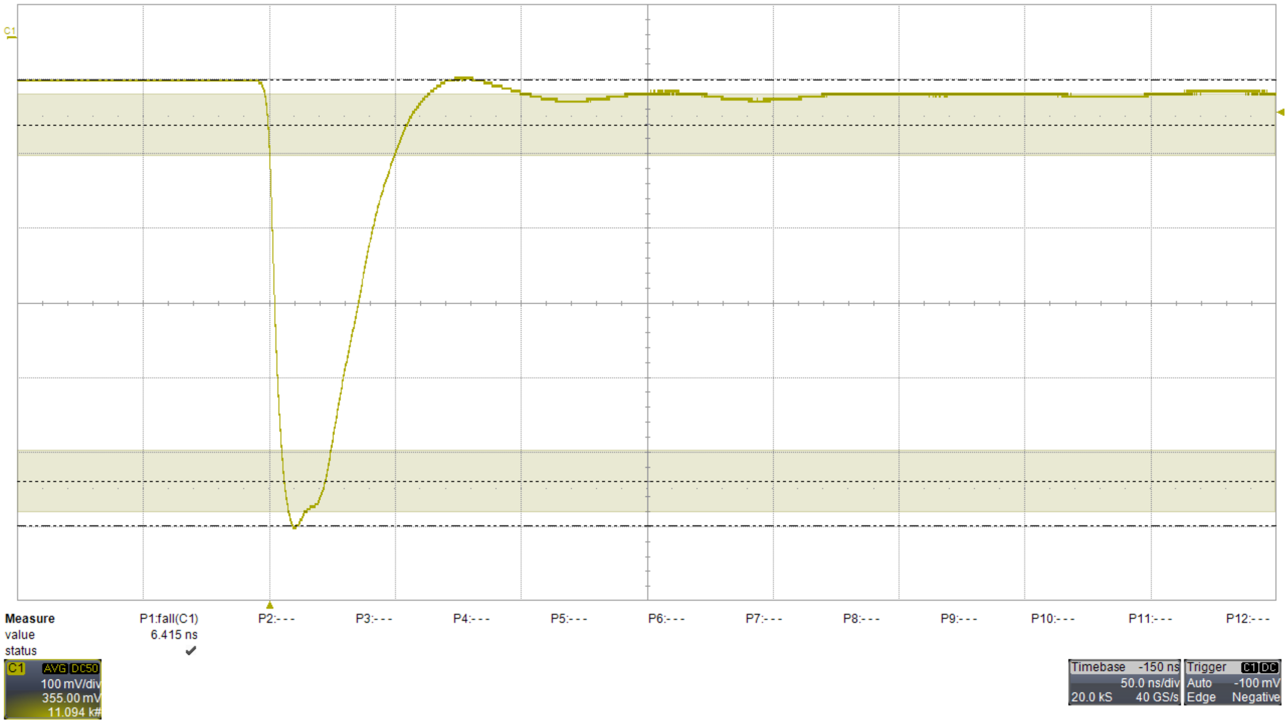

Measure	P1:fall(C1)	P2:- - -	P3:- - -	P4:- - -	P5:- - -	P6:- - -	P7:- - -	P8:- - -	P9:- - -	P10:- - -	P11:- - -	P12:- - -
value	6.415 ns											
status	✓											

C1 AVG DC50
100 mV/div
355.00 mV
11.094 k#

Timebase -150 ns
50.0 ns/div
20.0 kS 40 GS/s

Trigger C1 DC
Auto -100 mV
Edge Negative

Figure 22. Average response of SiPM array to a laser pulse, as determined by AiT Instruments. The laser pulses were 5 ns, much shorter than the typical response timing of the SiPM array and readout board itself. We see that while there is no overshoot, there is a long tail lasting hundreds of microseconds. The PSD analysis does not distinguish between this readout-based tail and the light tail from the detector material itself. The effect is to shift effective light production from both neutron and gamma recoils to later times, obscuring the PSD separation of the two kinds of bands.

performed with smaller crystals and smaller SiPM arrays[9,10]. Other readout board designs, optimized for the best combination of unipolar response and shortest return to baseline, should increase the PSD performance of the SiPM array. To this end we have begun working with CAEN SpA to develop a readout board for the SiPM array.

CONCLUSIONS

For the purposes of gamma ray spectroscopy and uranium enrichment measurements, we have determined that silicon photomultiplier arrays are a viable substitution for photomultiplier tubes. Because the uranium enrichment determination is based on the acquired spectra, we feel confident that other scintillator-based nuclear safeguards instrumentation would also be able to utilize SiPM arrays instead of PMTs. Of key importance in replacing PMTs with SiPMs is the choice in readout board, as some boards have been optimized for fast response while others are optimized for low noise levels.

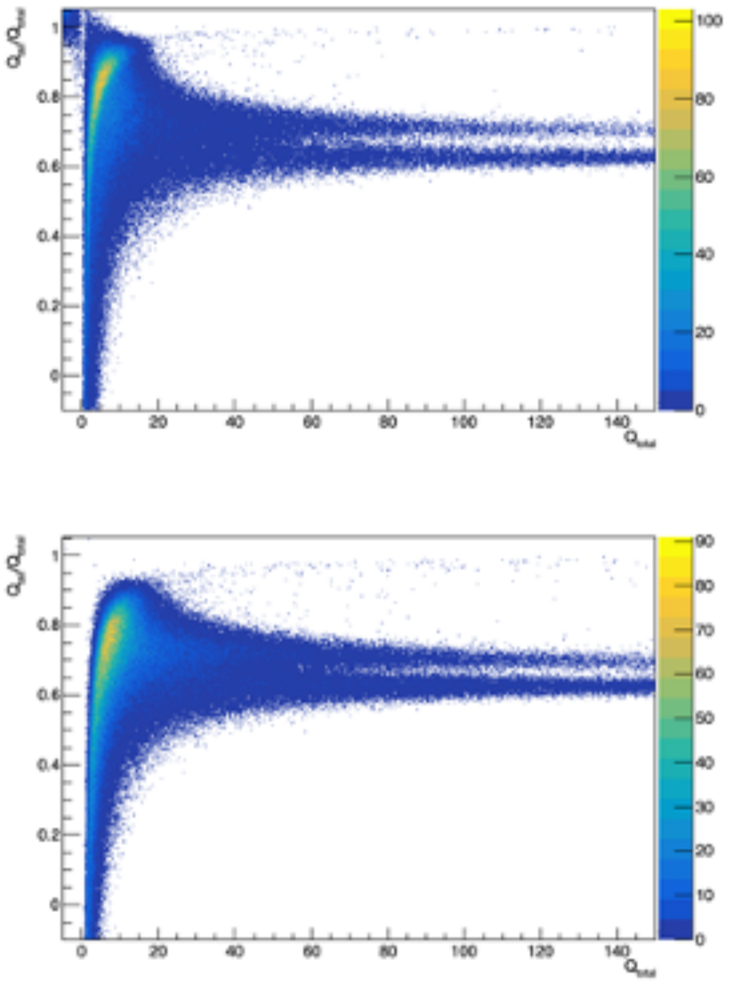

Figure 23. Optimized neutron and gamma bands from the SiPM array mounted to the the stilbene cylinder (top) and square detector (bottom). The maximum Figure of Merit was 2.8 for the cylinder and 3.4 for the square. This is to be compared to a FOM pdf 6.6 for the PMT mounted to the cylinder.

For neutron detection, we note that other groups have demonstrated the usefulness of SiPM-mounted organic scintillators, and there is therefore no fundamental incompatibility between SiPMs and pulse shape discrimination. Currently, however, there is only one commercial solution available to create a 4” × 4” array of SiPMs with a single channel output and a single power supply. That solution exhibits large electronic baseline noise relative to the PMT, which degrades the PSD capabilities. With a redesign of the readout board that focuses on reducing noise levels while maintaining sufficiently quick response, the PSD capabilities may be enhanced to the point that the SiPMs exhibit comparable PSD capabilities as the PMTs.

ACKNOWLEDGMENTS

We would like to thank Vladimir Mozin and Phil Kerr of Lawrence Livermore National Laboratory for their assistance in obtaining the uranium spectroscopy data. This work was supported by the U.S. Department of Energy, National Nuclear Security Administration, Office of Nonproliferation and Arms Control, International Nuclear Safeguards Technology Development and the Human Capital Development Programs. Prepared by LLNL under Contract DE-AC52-07NA27344. LLNL-TR-815543.

REFERENCES

---

[1] *Safeguards Techniques and Equipment: 2011 Edition*, IAEA/NVS/1/2011 (Rev. 2), International Atomic Energy Agency, Vienna (2011).

[2] S.C. Curran & W.R. Baker, “Photoelectric Alpha-Particle Detector”, *The Review of Scientific Instruments*, **19**(2), (1948) p. 116. The pairing of a scintillator and a photomultiplier tube are commonly attributed to Curran and Baker in 1944, though the authors of this current work were not able to review the original publication: S.C.Curran & W.Baker, Radiation Laboratory Report 7.6.16, November 17, Contract W-7405-eng-48, *Manhattan Project* (1944).

[3] Creative Commons Attribution-Share Alike 3.0 Unported, https://creativecommons.org/licenses/by-sa/3.0/deed.en. Attributed to Qwerty123uiop.

[4] K. Kazkaz & E. Swanberg, “Survey of Current and Future PMT Replacement Technology”, Lawrence Livermore National Laboratory Technical Report, LLNL-TR-759403 (2018).

[5] NBL Certified Reference Materials CATALOG, New Brunswick Laboratory, December 2002.

[6] J. K. Sprinkle, Jr., et al., “Low-resolution gamma-ray measurements of uranium enrichment”, *Los Alamos National Laboratory*, Report LA-UR-96-3484 (1996).

[7] P. Mortreau & R. Berndt, “Determination of the uranium enrichment with the NaIGEM code", *Nuclear Instruments and Methods in Physics Research A,* **530** (2004) p.559–567.

[8] J. Allison et al., “Recent developments in GEANT4”, *Nuclear Instruments and Methods in Physics Research A*, **835** (2016) p.186-225.

[9] M.L. Ruch, M. Flaska, S.A. Pozzi, “Pulse shape discrimination performance of stilbene coupled to low-noise silicon photomultipliers”, *Nuclear Instruments and Methods in Physics Research A*, **793** (2015) p.1-5.

[10] M. Sweany, P. Marleau, C. Allwork, G. Kallenbach, S. Hammon, “Characterization of a silicon photo-multiplier array with summing board as a photo-multiplier tube replacement in organic scintillator assemblies”, *Nuclear Instruments and Methods in Physics Research A*, **953** (2020) 163118.